Journal of Power Sources 191 (2009) 275–279

Contents lists available at ScienceDirect

Journal of Power Sources

journal homepage: www.elsevier.com/locate/jpowsour

Short communication

Microstructure, oxygen stoichiometry and electrical conductivity of flame-sprayed $Sm_{0.7}Sr_{0.3}CoO_{3-\delta}$

Min Gao[a,b], Chang-Jiu Li[a,*], Cheng-Xin Li[a], Guan-Jun Yang[a], Sheng-Qiang Fan[a]

[a] State Key Laboratory for Mechanical Behavior of Materials, School of Materials Science and Engineering, Xi'an Jiaotong University, Xianning Wertern Road 28, Xi'an, Shaanxi 710049, PR China
[b] School of Material Science and Engineering, Georgia Institute of Technology, Atlanta, GA 30332-0245, USA

ARTICLE INFO

Article history:
Received 4 February 2009
Accepted 9 February 2009
Available online 20 February 2009

Keywords:
Solid oxide fuel cells
Cathode
$Sm_{0.7}Sr_{0.3}CoO_{3-\delta}$
Flame spraying

ABSTRACT

A SSC deposit has been prepared by flame spraying using $Sm_{0.7}Sr_{0.3}CoO_{3-\delta}$ (SSC) powder synthesized by a solid-state reaction. A post-spray annealing treatment of the SSC deposit has been performed. The coating characterization includes: the electrical conductivity of the SSC deposit along the lamellar direction measured by a four-electrode D.C. approach, the microstructures of SSC powders and deposits characterized using X-ray diffraction and scanning electron microscopy, the oxygen stoichiometry in both the as-sprayed and annealed deposits and starting powder determined by redox titration. The results show that a significant oxygen deficiency (12%) occurs in the sprayed powder particles during high temperature flame spraying, leading to reduction of the electrical conductivity of the as-sprayed SSC deposit. It is found that oxygen can be recovered through post-spray annealing treatment. After annealing at 900 °C for 5 h or at 1100 °C for 10 h, the electrical conductivity of annealed SSC reaches 433 S cm^{-1} or 510 S cm^{-1} at 600 °C due to a sharp recovery of deficient oxygen and microstructural change.

1. Introduction

Solid oxide fuel cells (SOFCs) are highly efficient and environmentally friendly power-generating systems that convert the chemical energy of hydrogen or other fuels directly into electrical energy through an electrochemical reaction with oxygen [1]. The major obstacles for commercial application of SOFCs are high manufacturing cost and limited performance, both in terms of materials and processing.

For intermediate temperature solid oxide fuel cells (IT-SOFCs) operated below 800 °C, inexpensive interconnects and sealing materials can be utilized and some high temperature complications such as densification of electrodes, formation of an insulating layer at the electrode/electrolyte interface by inter-diffusion, and crack formation induced by stress caused by large differences in the thermal expansion coefficients of the cell components can be avoided [2]. However, at reduced operating temperatures, polarization of the traditional Sr-doped $LaMnO_3$ (LSM) cathode becomes a critical problem for the IT-SOFC cell performance as the operating temperature decreases [3].

Studies show that cobalt-containing perovskite-type oxides are suitable to be used as the cathode materials for intermediate temperature SOFCs due to their relatively large ionic conductivity [4–6]. Among them, $Sm_xSr_{1-x}CoO_3$ (SSC) is regarded as one of the most promising cathode materials owing to its high degree of mixed electronic and ionic conductivity. Recently, several studies have been focused on methods of synthesizing SSC, such as solid-state reaction, sol–gel methods and the glycine–nitrate process [7–10] as well as on SSC composite cathodes consisting of SSC–$La_{0.8}Sr_{0.2}Ga_{0.8}Mg_{0.2-x}Co_xO_3$ (LSGMC) [11], SSC–$Gd_{0.1}Ce_{0.9}O_{1.95}$ (GDC) [12], SSC–samaria-doped ceria (SDC) [13–15] and SSC–$Ba(Zr_{0.1}Ce_{0.7}Y_{0.2})O_{3-\delta}$ (BZCY) [16]. A study on the reaction model of $Sm_{0.5}Sr_{0.5}CoO_3$ cathode was carried out by Fukunaga et al. [17]. Crystal structure, thermal expansion coefficient, electrical conductivity and cathode polarization of $Sm_{0.5}Sr_{0.5}Co_{1-x}Fe_xO_{3-\delta}$ (SSCF) ($0 \le x \le 0.9$) series have also been studied by Lv et al. [18].

Additionally, commercialization efforts for SOFC systems have been recently focused on reducing manufacturing cost. Thermal spraying is considered to be a promising processing method because of its fast deposition rate and cost-effectiveness compared with other film formation processes [19]. Atmospheric plasma spray (APS) has been applied for the preparation of the anode [21,24], electrolyte [22–25], cathode [23–26] and interconnect component [20,21]. Applying APS, a fuel cell with 30 μm electrolyte,

* Corresponding author. Tel.: +86 29 82660970; fax: +86 29 83237910.
E-mail address: licj@mail.xjtu.edu.cn (C.-J. Li).

0378-7753/$ – see front matter © 2009 Elsevier B.V. All rights reserved.
doi:10.1016/j.jpowsour.2009.02.016

30–50 μm anode and cathode was designed by Schiller et al. and successfully operated under 800 °C [27,28].

However, few papers are concerned with the features of thermally sprayed SSC. In this paper, $Sm_{0.7}Sr_{0.3}CoO_3$ (SSC) deposit was prepared by flame spraying and post-spray annealing of the SSC deposit was carried out under air atmosphere at 900 °C for 5 h and at 1100 °C for 10 h. The microstructure, oxygen stoichiometry and electrical conductivity of the both as-sprayed and annealed SSC were characterized. The influence of oxygen stoichiometry and microstructure of the SSC deposits on the electrical conductivity was examined.

2. Experimental

The proper amounts of Sm_2O_3, $SrCO_3$ and Co_2O_3 to obtain the composition $Sm_{0.7}Sr_{0.3}CoO_3$ (SSC) were weighed and mixed in a beaker. Using alcohol as mediator, the mixture was ground in a mortar for 2 h to obtain a homogeneous slurry. The slurry was dried in a drying oven at 100 °C to evaporate the alcohol. Then, the dry mixture was ground again and calcined at 1200 °C for 20 h. A grey bulk was obtained and the products were characterized by X-ray diffraction (XRD-6000, Shimadzu).

The SSC bulk was then crushed and sifted to a proper particle size range, 50–100 μm, for spraying. Using a commercial flame spraying system (HP-2000, Dahao Inframet, Shanghai), with the pressures of oxygen and acetylene being 0.5 MPa and 0.09 MPa, respectively, an SSC deposit was prepared using the following procedure. First, a layer of salt was deposited on the stainless steel substrate. Second, a 3 mm layer of SSC was deposited on the salt. Third, the coating and substrate were cooled to room temperature and then put into distilled water. A free-standing SSC deposit was separated from the substrate when the salt was totally dissolved.

The post-spray annealing treatment of the SSC deposit was carried out at 900 °C for 5 h or at 1100 °C for 10 h. The crystalline structures of both the as-deposited and annealed SSC deposit were investigated by X-ray diffraction (XRD-6000, Shimadzu), using Cu Kα radiation within a 2θ range 10–80° in a step of 0.02°. Surface morphology and cross-sectional microstructure of the SSC deposits were characterized by scanning electron microscopy (Quanta 200, Dutch).

The oxygen stoichiometry in both the as-sprayed and annealed deposits and starting powder was determined by redox titration. First, 100 mg of accurately weighed dry $Sm_{0.7}Sr_{0.3}CoO_{3-\delta}$ powder was placed in a conical flask. Second, the sample was dissolved in 25.00 ml acidified, 0.0991 mol L^{-1} Fe (II) sulfate solution. The ferrous ion reduced all cobalt to the Co (II) state. Then, the amount of Fe (II) left over was titrated by standardized 0.0252 mol L^{-1} $K_2Cr_2O_7$ solution to purple in the presence of sodium diphenylaminesulfonate as an indicator, and 30 mL mixture of sulfuric acid and phosphoric acid was added into the solution at the same time to enlarge the titration jump.

For $Sm_{0.7}Sr_{0.3}CoO_{3-\delta}$, it was assumed that Sm^{3+}, Sr^{2+} and O^{2-} take fixed valence. The mean valence of the cobalt ion is $3+p$ assuming a charge neutrality condition.

The chemical reaction follows two steps. The first reaction occurs as:

$$(1+p)Fe^{2+} + Co^{3+p} \rightarrow (1+p)Fe^{3+} + Co^{2+}$$

From this reaction, the following relationship can be obtained:

$$\frac{n_{Fe^{2+}}}{(1+p)} = n_{Co^{3+p}} = \frac{W}{M} \quad (1)$$

where $n_{Fe^{2+}}$ and $n_{Co^{3+p}}$ are the Moore number of reacted Fe^{2+} and the reacted Co^{3+p}, respectively, W is the mass of the $Sm_{0.7}Sr_{0.3}CoO_{3-\delta}$ sample, M is the molar mass of the $Sm_{0.7}Sr_{0.3}CoO_{3-\delta}$ sample.

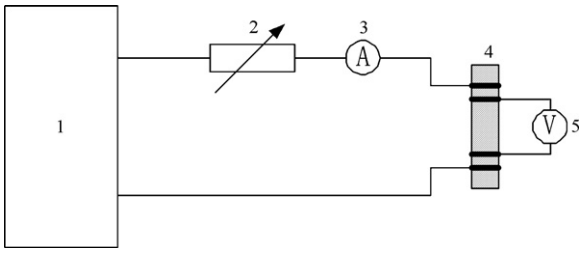

Fig. 1. Schematic of four-probe method. (1) DC power source, (2) resistance, (3) ammeter, (4) SSC sample, (5) voltage meter.

Then, the remaining Fe^{2+} is titrated by the standardized $K_2Cr_2O_7$ as follows:

$$14H^+ + Cr_2O_7^{2-} + 6Fe^{2+} \rightarrow 2Cr^{3+} + 6Fe^{3+} + 7H_2O$$

After the complete reaction, the remaining Fe^{2+} can be calculated:

$$n_{Fe^{2+}}(\text{remaining}) = 6c_{K_2Cr_2O_7}V_{K_2Cr_2O_7}$$

where $c_{K_2Cr_2O_7}$ is the concentration of the standardized $K_2Cr_2O_7$ solution and $V_{K_2Cr_2O_7}$ is the consumed volume of the $K_2Cr_2O_7$ standard solution.

The Moore number of Fe^{2+} reacted with Co^{3+p} is equal to the total Moore number of Fe^{2+} minus that of remaining Fe^{2+}:

$$\begin{aligned} n_{Fe^{2+}} &= 10^{-3}[25.00c_{Fe^{2+}} - n_{Fe^{2+}}(\text{remaining})] \\ &= 10^{-3}(25.00c_{Fe^{2+}} - 6c_{K_2Cr_2O_7}V_{K_2Cr_2O_7}) \end{aligned} \quad (2)$$

where $c_{Fe^{2+}}$ is the concentration of the standardized Fe^{2+} solution.

p is related to δ as follows:

$$p + 2\delta = 0.3 \quad (3)$$

In addition:

$$M = M_0 - 15.999\delta = 238.54 - 15.999\delta \quad (4)$$

where M_0 is molar mass of the $Sm_{0.7}Sr_{0.3}CoO_3$.

Substituting (2)–(4) into (1), δ is determined:

$$\delta = \frac{1.3W - 238.54 \times 10^{-3}(25.00c_{Fe^{2+}} - 6c_{K_2Cr_2O_7}V_{K_2Cr_2O_7})}{2W - 15.999 \times 10^{-3}(25.00c_{Fe^{2+}} - 6c_{K_2Cr_2O_7}V_{K_2Cr_2O_7})}$$

The electrical conductivities of the SSC deposits were measured using four-probe D.C. method, the schematic of which is shown in Fig. 1. Before testing, four platinum wires were adhered to the sample with platinum paste. Direct current was applied to the outer

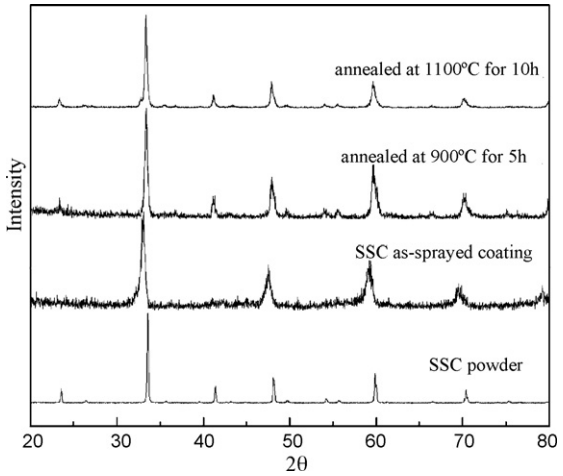

Fig. 2. XRD patterns of SSC.

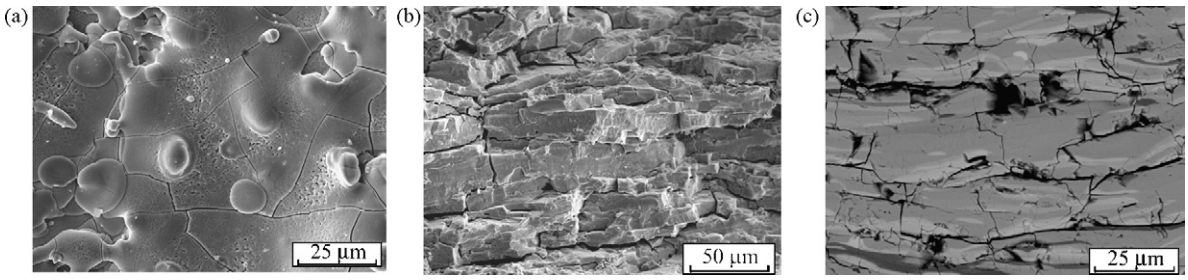

Fig. 3. Typical surface topographical morphology of the as-sprayed SSC (a), and morphology of the fractured SSC coating (b) and cross-sectional microstructure of the as-sprayed SSC (c).

two wires and the voltage was measured between the inner two wires.

The weight change of the sample was investigated up to 1000 °C using a thermogravimetric apparatus (SDT Q600, USA). The sample mass was around 50 mg and the sample was heated in air atmosphere at a heating rate of 5 °C min^{-1}.

3. Results and discussion

3.1. Morphology and microstructure of the SSC deposits

XRD patterns of the SSC powder, as-sprayed SSC deposit and annealed deposit are shown in Fig. 2. The starting SSC powder was a pure perovskite phase. After spraying, the peaks in the XRD pattern were noticeably broadened, which implies that fine crystalline grains were present in the as-sprayed deposit. A slight shift of XRD peaks suggested a distortion of the lattice in the as-sprayed deposit. Thermal spray deposit is generally deposited through rapid splat cooling process. After annealing, the shift of XRD peaks disappeared and the peak width narrowed, suggesting a decrease of stress and increase in crystal size.

Fig. 3 shows the typical surface morphology and cross-sectional microstructure of the as-sprayed SSC deposit. The SSC deposit exhibited a typical morphology of well-spread splats (Fig. 3a). This fact indicates that the deposit was formed from sufficiently melted spray particles and was confirmed by the lamellar structure revealed by the fractured cross-section of the SSC deposit as shown in Fig. 3b. The microstructure of the polished cross-section of the deposit (Fig. 3c) demonstrated some voids present in the deposit, which appear with a black contrast. Moreover, many microcracks were present in the splats (Fig. 3a) and lamellar voids, which are referred to as the nonbonded lamellar interface [29], were observed in the fractured deposit (Fig. 3b). All of these defects including large voids, microcracks and nonbonded interface areas constitute tunnels, which are interconnected, allowing for gas transport. The estimation through image analyzing from coating cross-section yielded a mean porosity level of 24% for the as-sprayed coating.

Fig. 4 shows the fractured coating cross-sectional morphology and polished cross-sectional microstructure after the coating was annealed at 900 °C for 5 h. It seems that sintering occurred to certain extent, which made the lamellar structure of the coating become less distinct (Fig. 4a). The sintering effect possibly leads to the coalescence of small voids including microcracks and nonbonded interface region, which resulted to the appearance of large voids present in the coating as shown in Fig. 4b. The large voids interconnected with cracks perpendicular to lamellar direction can act as a path for cathode gas.

Fig. 5 shows the cross-sectional morphology of the deposit annealed at 1100 °C for 10 h. The lamellar voids and microcracks were still observed, indicating limited sintering. Moreover, the number of voids became decreased and the volume of single voids become larger than that of the as-sprayed sample, possibly due to the coalescence of small voids and shrinkage of the deposit resulting from sintering. This fact implies that the sintering leads to the redistribution of voids and formation of large tunnels perpendicular to lamellae, which is beneficial for gas transportation during operation as a cathode.

3.2. Oxygen content in the as-sprayed and the annealed SSC deposits

The TGA curves of SSC powder and the SSC deposit are shown in Fig. 6. The weight of the starting SSC powder decreased with the increase of temperature from room temperature to 1000 °C, indicating the loss of oxygen from the SSC lattice at high temperature, especially at temperature higher than 700 °C. The as-sprayed SSC deposit (Fig. 6b) exhibited a different dependence of weight change on temperature from the starting powder (Fig. 6a). The weight of SSC deposit increased with the increase of temperature from room temperature to about 930 °C. Although the weight of SSC deposit began to decrease with increasing temperature from 930 °C, the net weight of sample at high temperature was increased compared with the sample weight at room temperature. The different behavior of the as-sprayed SSC from the starting powder is attributed

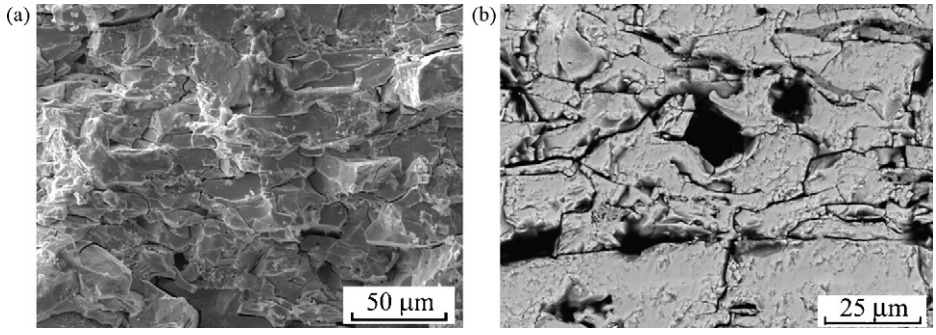

Fig. 4. Cross-sectional microstructure of SSC coatings annealed at 900 for 5 h. (a) Morphology of the fractured SSC coating and (b) cross-sectional microstructure of the annealed SSC coatings.

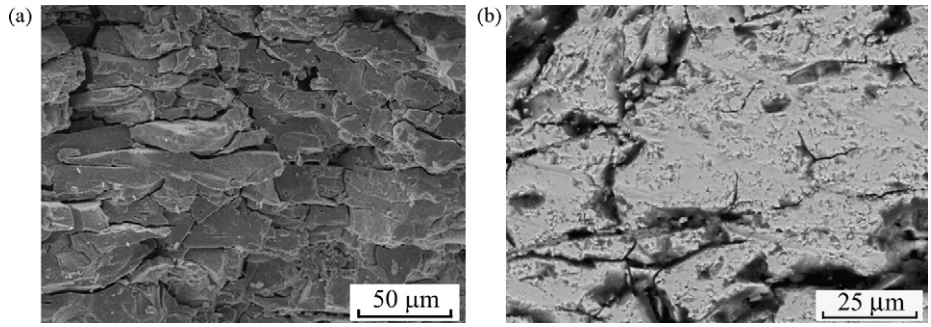

Fig. 5. Cross-sectional microstructure of SSC coatings annealed at 1100 for 10 h. (a) Morphology of the fractured SSC coating and (b) cross-sectional microstructure of the annealed SSC coatings.

to the oxygen loss occurring in in-flight powder particles during spraying.

The oxygen contents in the SSC samples determined by redox titration are shown in Table 1. The oxygen deficiency, δ, in the starting powder, as-sprayed SSC, SSC deposit annealed at 900 °C for 5 h, and SSC coating annealed at 1100 °C for 10 h were 0.17, 0.37, 0.18 and 0.14, respectively. It is clear that the oxygen deficiency of SSC after passing through the high temperature flame increased, leading to the formation of the SSC deposit with large nonstoichiometry of oxygen, which amounted 12% of the total oxygen. High temperature annealing of the as-sprayed SSC led to rapid recovery of oxygen content. After annealing at a temperature of 900 °C for 5 h, the oxygen content recovered to the level comparable to that of the starting powder. Moreover, the oxygen recovery at high temperature was responsible for the difference in the TGA curve of the SSC powder from that of the as-sprayed SSC.

Table 1
The oxygen contents of SSC.

SSC sample	m (mg)	$V_{K_2Cr_2O_7}$ (mL)	δ	Average δ
SSC powder	114.7	13.38	0.16	0.17
	131.8	12.97	0.17	
	137.6	12.84	0.17	
As-sprayed SSC deposit	126.0	14.50	0.37	0.37
	113.0	14.70	0.37	
	90.6	15.08	0.37	
Annealed SSC deposit (at 900 °C for 5 h)	136.5	12.93	0.18	0.18
	102.1	13.84	0.18	
	116.8	13.40	0.17	
Annealed SSC deposit (at 1100 °C for 10 h)	134.4	12.70	0.14	0.14
	120.6	13.10	0.14	
	103.4	13.59	0.14	

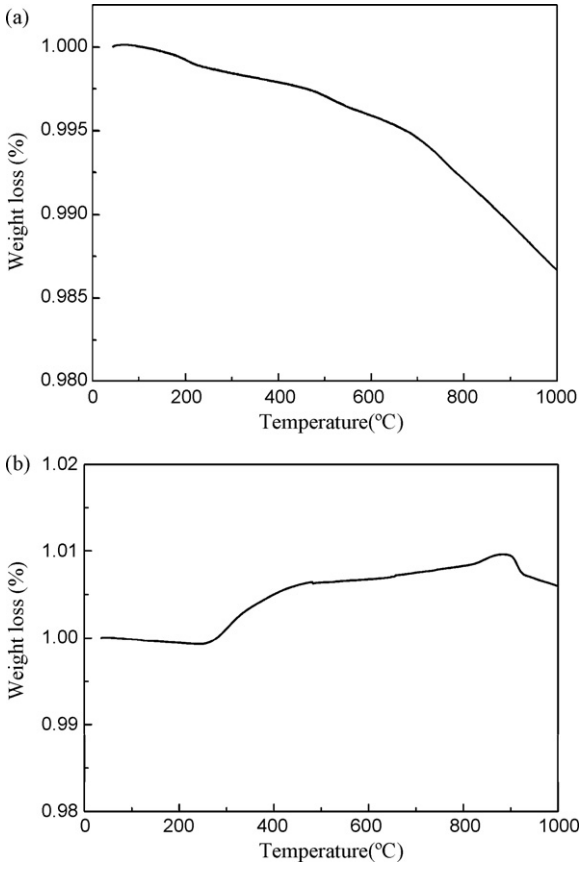

Fig. 6. TGA curve of SSC powder (a) and SSC deposit (b).

3.3. Electrical conductivity of the SSC deposit

The temperature dependence of the electrical conductivity of the as-sprayed and annealed SSC deposits is shown in Fig. 7. The conductivity of the as-sprayed SSC increased with temperature from room temperature to about 1000 °C. However, the value of electrical conductivity was lower than that reported for the sintered bulk [7]. The conductivity of the annealed SSC increased with temperature from room temperature to about 600 °C, and then decreased with further increases in temperature above 600 °C. This trend is similar to that of SSC bulk [7]. The maximum electrical conductivity of the annealed SSC deposit reached 433 S cm^{-1} and 510 S cm^{-1} at about 600 °C after annealing at 900 °C for 5 h and at 1100 °C for 10 h.

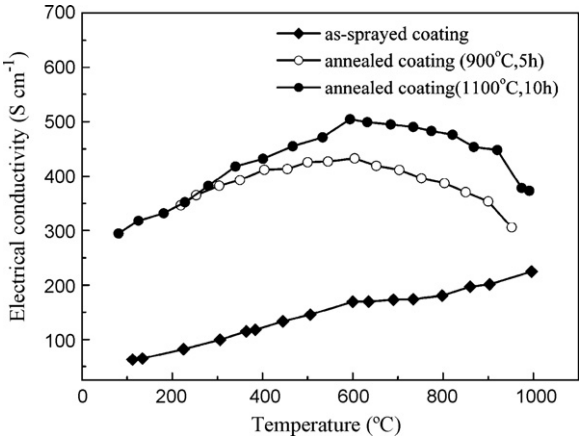

Fig. 7. Dependence of the electrical conductivity on test temperature of both the as-sprayed SSC and annealed SSC.

For doped SSC, the charge is compensated in two ways assuming localized charge carriers: (1) changing valences of the Co^{3+} ions to produce electron holes or electrons, and (2) producing oxygen vacancies. During thermal spraying, a loss of oxygen from the lattice and creation of oxygen vacancies occurred due to the exposure of SSC to high temperature flame. With data shown in Table 1, using Eq. (3), for as-sprayed SSC deposit, $p = -0.44$ and the mean valence of Co was 2.56. This shows that Co actually presents valence between II and III in SSC coating due to loss of oxygen and formation of a large number of oxygen vacancies in reduced flame and that the conduction by majority carrier was n-type and that of the minority carrier was p-type. For the coating annealed at 900 °C for 5 h, $p = -0.06$, so the mean valence of Co was 2.94. These facts indicate that the mean valence of Co increased with decrease of oxygen vacancy and that the number of p-type carriers increased. For the coating annealed at 1100 °C for 10 h, $p = 0.02$ and the mean valence of Co became 3.02. These results indicate that Co actually presents valence between III and IV in SSC coatings and the number of p-type carrier continued to increase.

According to hopping model, oxygen vacancies can reduce the number of p-type charge carriers and the electronic charge carrier mobility by acting as electron traps [30–32]. It was found that the recovery of deficient oxygen in the SSC deposit during annealing was significant, as δ decreased from 0.37 to 0.18 and 0.14. Therefore, it is possible that the p-type charge carrier concentration increased and n-type charge carrier concentration decreased while the oxygen vacancy concentration decreased, leading to a net increase in electronic charge carriers. This is possibly the one reason for the significant increase of the electrical conductivity of the annealed SSC deposit compared with the as-sprayed one.

Annealing also healed some of the voids including microcracks and nonbonded interface areas, resulting in more paths for the conduction of electronic species, contributing to the increase of electrical conductivity. In addition, some specific voids including microcracks and nonbonding areas existed in the as-sprayed lamellar SSC deposit (Fig. 3a–c), which may have been responsible to low electrical conductivity of the as-sprayed deposit compared with that of bulk SSC [7].

It can be clearly observed that the dependence of the electrical conductivity of the as-sprayed SSC was different from those of the annealed SSC and bulk SSC as well. This fact is attributed to the significant oxygen recovery of the as-sprayed SSC deposit at the elevated temperature. During measurement of the electrical conductivity for the as-sprayed SSC, the oxygen recovery became more intensive as the temperature increased to over 600 °C, which resulted in the increase in conductivity above 600 °C. However, the annealed coating exhibited an electrical conductivity much less than the sintered bulk. This is attributed to the lamellar features with limited interfacial bonding, which were not sufficiently healed under the present annealing conditions.

4. Conclusions

The flame-sprayed SSC exhibited a typical lamellar structure. Voids including microcracks and nonbonded interface areas were present in the deposit, providing passage for reaction gas. The results indicated that a significant oxygen deficiency occurred in sprayed powder particles, which experienced melting during spray process, and the rapid splat cooling retained the oxygen deficient state of SSC droplets into the deposit. An oxygen deficiency of about 12% was present in the present flame-sprayed SSC. As a result, the conductivity of the as-sprayed SSC increased with the increase of the temperature from room temperature to about 1000 °C. The conductivity of the annealed SSC increased with temperature until about 600 °C and then decreased with further increase of temperature above 600 °C. The annealing treatment led to the oxygen recovery of the as-sprayed SSC deposit and increased the electrical conductivity of the SSC deposit. The maximum electrical conductivity of the annealed SSC at 600 °C and 1100 °C reached 433 S cm^{-1} or 510 S cm^{-1}, respectively. The low electrical conductivity of the annealed SSC deposit in comparison with the sintered bulk is attributed to the characteristic voids in the sprayed SSC deposit. The SSC deposit can be further optimized through compromising of the electrical conductivity and deposit voids for gas transfer by changing the spraying parameters such as gas flow, stand off distance and flame power.

Acknowledgements

The present project was supported by National Technology Research and Development Program of China (Granted No. 2007AA05Z135) and National Natural Science Funds for Distinguished Young Scholar (Granted No. 50725101). The author thanks Matt Lynch of the school of Materials Science and Engineering, Georgia Institute of Technology, for his comments and suggestions.

References

[1] O. Yamamoto, Electrochim. Acta 45 (2000) 2423–2435.
[2] E. Ivers-Tiffee, et al., J. Eur. Ceram. Soc. 21 (2001) 1805–1809.
[3] B.C.H. Steels, A. Heinzel, Nature 414 (2001) 345–352.
[4] B.C.H. Steele, Solid State Ionics 129 (2000) 95–110.
[5] E. Maguire, B. Gharbage, F.M.B. Marques, J.A. Labrincha, Solid State Ionics 127 (2000) 329–335.
[6] V. Dusastre, J.A. Kilner, Solid State Ionics 126 (1999) 163–174.
[7] H.Y. Tu, Y. Takeda, N. Imanishi, O. Yamamoto, Solid State Ionics 100 (1997) 283–288.
[8] N.P. Bansal, Z.M. Zhong, J. Power Sources 158 (2006) 148–153.
[9] S. Yang, T.M. He, Q. He, J. Alloys Compd. 450 (2008) 400–404.
[10] Z.L. Tang, Y.S. Xie, H. Hawthorne, D. Ghosh, J. Power Sources 157 (2006) 385–388.
[11] S.Z. Wang, T. Chen, S.P. Chen, J. Electrochem. Soc. 151 (9) (2004) A1461–A1467.
[12] C.R. Xia, M.L. Liu, Solid State Ionics 144 (2001) 249–255.
[13] C.R. Xia, W. Rauch, F.L. Chen, M.L. Liu, Solid State Ionics 149 (2002) 11–19.
[14] Y. Liu, W. Rauch, S.W. Zha, M.L. Liu, Solid State Ionics 166 (2004) 261–268.
[15] X.G. Zhang, M. Robertson, S. Yick, C. Dêces-Petit, E. Styles, W. Qu, Y.S. Xie, R. Hui, J. Roller, O. Kesler, R. Maric, D. Ghosh, J. Power Sources 160 (2006) 1211–1216.
[16] L. Yang, C. Zuo, S.Z. Wang, Z. Cheng, M.L. Liu, Adv. Mater. 20 (2008) 3280–3283.
[17] H. Fukunaga, M. Koyama, N. Takahashi, C. Wen, K. Yamada, Solid State Ionics 132 (2000) 279–285.
[18] H. Lv, Y.-J. Wu, B. Huang, B.-Y. Zhao, K.-A. Hu, Solid State Ionics 177 (2006) 901–906.
[19] C.-J. Li, C.-X. Li, Y.-Z. Xing, M. Gao, G.-J. Yang, Solid State Ionics 177 (2006) 2065–2069.
[20] T.-L. Wen, D. Wang, H.-Y. Tu, M. Chen, Z. Lu, Z. Zhang, H. Nie, W. Huang, Solid State Ionics 152–153 (2002) 399.
[21] T. Okuo, Y. Kaga, A. Momma, Denki Kagaku 64 (6) (1996) 555–561.
[22] S. Takenori, N. Kadokawa, K. Koseki, J. Therm. Spray Technol. 9 (2000) 360–363.
[23] C.-J. Li, C.-X. Li, X.-J. Ning, Vacuum 73 (2004) 699–703.
[24] R. Zheng, X.-M. Zhou, S.-R. Wang, T.-L. Wen, C.-X. Ding, J. Power Sources 140 (2005) 217–225.
[25] K. Okumura, Y. Aihara, S. Ito, S. Kawasaki, J. Therm. Spray Technol. 9 (2000) 354–359.
[26] K. Barthel, S. Rambert, S. Siegmann, J. Therm. Spray Technol. 9 (2000) 343–347.
[27] G. Schiller, R.H. Henne, M. Lang, Proceedings of the ITSC, Osaka, Japan, 2004, pp. 100–105.
[28] G. Schiller, H. Rudolf, M. Lang, Fuel cells Bull. 21 (2000) 7–12.
[29] X.-J. Ning, C.-J. Li, C.-X. Li, G.-J. Yang, Mater. Sci. Eng. A 428 (2006) 98–105.
[30] E. Bucher, W. Sitte, Solid State Ionics 173 (2004) 23–28.
[31] L.-W. Tai, M.M. Nasrallah, H.U. Anderson, D.M. Sparlin, S.R. Sehlin, Solid State Ionics 76 (1995) 273–283.
[32] E.N. Naumovich, M.V. Patrakeev, V.V. Kharton, M.S. Islam, A.A. Yaremchenko, J.R. Frade, F.M.B. Marques, Solid State Ionics 177 (2006) 457–470.